Mode-I Fracture Behaviors of a Shear Thickening Fluid as Adhesive Layer under Different Loading Rates

Maisha Tabassum[1], Lin Ye[1,*], Li Chang[1], Klaus Friedrich[2,3]

[1] Center for Advanced Materials Technology, School of Aerospace, Mechanical and Mechatronic Engineering, The University of Sydney, NSW, 2006, Australia
[2] Institute for Composite Materials, University of Kaiserslautern, 67663 Kaiserslautern, Germany
[3] College of Engineering, King Saud University, Riyadh, Saudi Arabia
* Email: lin.ye@sydney.edu.au

Abstract Shear thickening fluids (STFs) classified as Non-Newtonian fluids are fluidic composites of dense suspensions. These fluids display unusual phase transitions between liquid and "solid" phases due to recoverable changes in viscosity at a critical rate of shear. This study characterizes the fracture behavior of a STF with 58 vol.% dispersion of styrene/acrylate particles in ethylene glycol. Double cantilever beam (DCB) specimens with the STF as adhesive layer were utilized to investigate the Mode-I fracture energy of the STF. The fracture behavior of the STF of different thickness was evaluated in detail at different crack opening displacement rates, varying from 1 mm/s to 50 mm/s. The results indicate that the fracture behavior of the STF is very rate-sensitive. However, before the opening displacement rate reaches 5 mm/s, the STF is not showing any "solid" like behavior. The average Mode-I fracture energy of the STF increases with an increase in the opening displacement rate up to 30 mm/s, after that the values are plateaued and almost constant at 240 J/m^2. This is comparable to the fracture toughness of a typical epoxy. The fracture energy of the STF also shows an inverse dependence on the thickness of the STF at low opening displacement rates, but at high rates such dependence was not observed.

Keywords Fracture energy, Shear thickening fluid (STF), Rate effect, Double cantilever beam (DCB), Adhesive thickness

1. Introduction

The ability to divert or dissipate dynamic energy during impact has many engineering challenges in industrial, biomedical and military applications. Shear thickening fluids (STFs) can play a vital role in engineering designs as energy shunting materials. STFs are mostly fluidic composites of dense suspensions that exhibit reversible shear thickening behavior, and STFs are non-Newtonian fluids, which can sometime display intriguing phase transitions between liquid and "solid" phases due to the recoverable changes in viscosity at a critical shear rate [1]. The use of STFs opens up many opportunities in developing new passive, energy-absorbing systems in applications including liquid dampers/brakes, liquid armor, etc.

Over the last few decades, the shear thickening behavior of concentrated dispersions has been a major topic of interest for rheologists owing to their immense importance in industry [1-4]. Shear thickening was initially believed to be a severe problem, because it leads to such issues as failure of mixer motors due to overloading, damage mixer blade and other processing equipment, and induce dramatic changes in suspension microstructure, such as particle aggregation, which results in poor fluid and coating qualities [1]. The early investigations of shear thickening behavior were to mitigate damage on processing equipment caused by the shear thickening transition [5, 6]. Later STFs have become attractive due to their unique property that makes them ideal for energy absorption applications. When subjected to an impact, this shear rate-activated fluid converts from a low viscous to a high viscous state almost instantaneously, and it can absorb some of impact energy while helping to dissipate the remaining energy. Many studies have been done on the energy absorption applications of STFs. For the personal protection with application of STFs as 'liquid armor', it has attracted many efforts in research [1, 7-9], and STFs-treated fabrics showed not only

the enhanced ballistic resistance but also higher flexibility and light weight [10-17] than the untreated ones. STFs have been also used in several other specific applications, especially in ski boot cushioning, liquid couplings, shock absorber fillings, rotary speed limiters, damping and control devices [18, 19].

The previous studies clearly highlight the strong potential of STFs for various industrial applications as new adaptive energy-absorbing materials, owing to their unique mechanism of recoverable liquid-"solid" transitions. The performance of the STF-based systems is greatly dependent on the behavior of STFs near the shear thickening transition as well as their properties after the shear thickening transition in particular. Most existing research has focused on the characterization of STFs using classic rheological methodology. Previous research primarily dealt with examining the response of shear thickening systems, especially in the identification of critical transition which indicates shear thickening occurrence. However, the properties of STFs after the shear thickening transition cannot be captured because of the limitations of conventional rheometers.

In this study the fracture behavior of a STF composed of 58 vol.% dispersion of styrene/acrylate particles in ethylene glycol [20] was investigated to quantitatively evaluate the dilatant ability of STF to shunt energy after shear thickening transition. Virtually for all applications fracture toughness or fracture energy is one of the most important material properties for characterizing energy dissipation capability; and it can be dependent on several factors, such as the type of loading (e.g. tensile and shear), the environmental conditions (e.g. temperature and moisture), the loading rate. Fracture tests were performed using a double cantilever beam (DCB) specimen with STF as adhesive layer to investigate the effect of displacement rate and adhesive layer thickness. A high speed digital (HSD) camera was used to carefully examine the fracture behavior of STF.

2. Experimental

2.1. Material

The STF used in this research work is a water soluble fluid composed of 58 vol.% dispersion of styrene/acrylate particles in ethylene glycol, supplied by BASF AG (Germany). The spatial distribution and the geometry of particles have been examined previously using a Zeiss 902 transmission electron microscope (TEM) and a scanning electron microscope (SEM) [20], and the shape of particles is near-spherical with an average size of about 300 nm; the particles were well dispersed in the ethylene glycol with the existence of micro-sized flocculation.

2.2. Specimen Configuration

There is no standard method to measure the Mode-I fracture energy of STFs. In this work, double cantilever beam (DCB) specimens with the STF as the adhesive layer were adopted in such an approach. The upper and lower beams of DCB specimens were carbon fiber-epoxy (CF/EP) plain woven composite beams, which were selected owing to their high stiffness, lightweight and smooth surface properties. The CF/EP beam was 200 mm long with 30 mm in width and 1.7 mm in thickness. Two aluminium (Al) loading blocks were bonded on the upper and lower surface of CF/EP beams at one end using a high strength adhesive, as shown in Fig. 1.

Before applying the STF, the surfaces of CF/EP beams were cleaned by rinsing with water. After water rinsing and complete drying, STF was uniformly distributed between two beams with a folded Al foil of 0.02 mm in thickness, which replicates a single entity of a start-crack (Fig. 1). The

length of the start-crack amounted to 50 mm. The folded Al foil was chosen to form the start-crack due to its flexibility, thin and smooth surface features. To maintain the uniform thickness of the adhesive layer without voids in it, sufficient STF needs to be applied to allow a continuous spreading of the STF from the center of the specimen to the edges by squeezing flow. Different adhesive layer thicknesses, ranging from 0.2 mm to 2.05 mm, were obtained for the Mode-I fracture experiments.

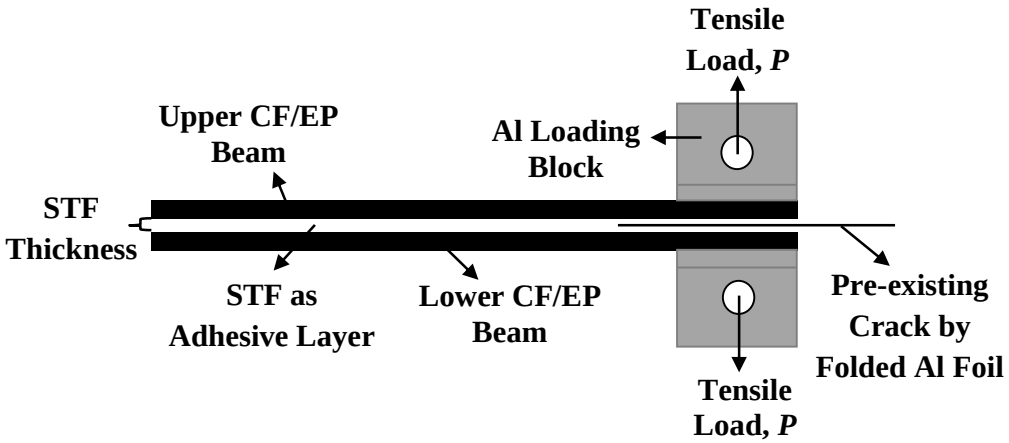

Figure 1. Schematic diagram of a DCB specimen with STF as adhesive layer and Al foil as a pre-existing crack

2.3. Mode-I Fracture Test Procedure

An Instron 8501 servo-hydraulic machine configured with a data acquisition system was utilized to conduct experiments in a displacement-controlled mode. The load experienced throughout the experimental duration with respect to the crack opening displacement was monitored and recorded through the load cell by a digital data acquisition unit at a sampling rate of 1000 Hz. Experiments were performed under various stroke speeds, ranging from 1 to 50 mm/s for the DCB specimens with different STF thickness, while holding all other variables constant. Stroke speeds chosen for experiments were 1, 5, 10, 20, 30, 40, and 50 mm/s, and all tests were undertaken under ambient conditions. Up to 50 experiments were conducted at each displacement rate with different STF thickness.

2.4. High-Speed Photography

Video recording was performed during each experiment using a high speed digital (HSD) camera with a frame rate of 500 frames/sec (fps) at a resolution of 512 ×240 pixels per image, in order to capture the specimen's physical movement. It helped to calibrate the actual displacement, and it also helped to observe the crack opening and crack propagation. With the help of a software program, the fracture behavior of STF in different stages of loading could be evaluated in detail.

2.5. Fracture Energy

The fracture energy of the STF to resist opening separation can be established by accessing the raw data obtained from the experiments. Continuous records of HSD image, load and corresponding opening deflection of CF/EP beams were used for determination of the fracture energy of STF in a DCB specimen. The data reduction scheme to determine the fracture energy for the DCB specimen with an adhesive layer of STF is the 'Modified Beam Theory (MBT) Method' [21] which quantifies the strain energy release rate at the crack initiation and propagation. The fracture energy or the critical energy release of a DCB specimen [22] is expressed as:

$$G_I = \frac{3P_c\delta_c}{2ba} \quad (1)$$

where, P_c = the critical load for crack growth, δ_c = the opening displacement at the critical load P_c, b = the specimen width, and a = the start-crack length.

3. Results and Discussion

3.1. Fracture Load

The response of the STF undergoing DCB fracture test was quantitatively assessed by synchronizing the load experienced by DCB specimen against its opening deflection in conjunction with the records of the HSD camera. Fig. 2 shows the typical load-displacement curve at a displacement rate of 40 mm/s. At point O_1, a local hike in load can be observed, but no crack growth was clearly visible in the specimen, Fig. 3(a). When the load was further increased, reaching its peak, point O_2, a white spot was observed in the STF layer at the tip of the start-crack, Fig. 3(b), showing the initiation of crack growth. After the peak, point O_2, the load started to drop continuously, accompanied by crack propagation in the specimen, Fig. 3(c).

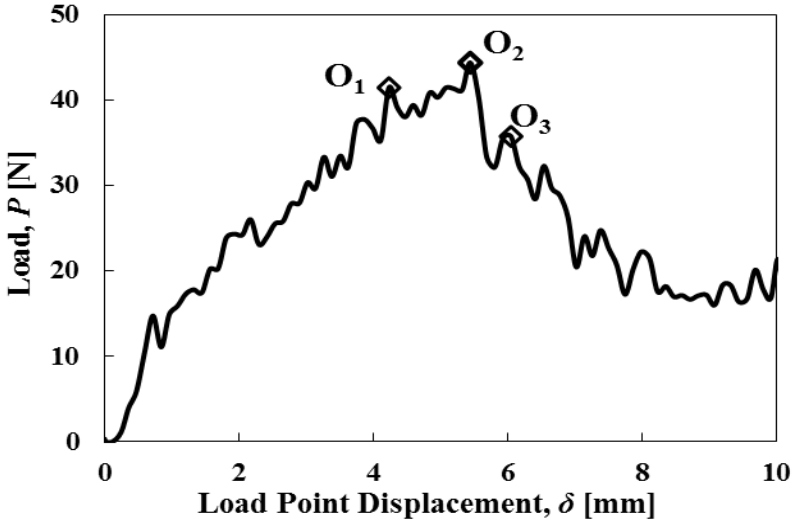

Figure 2. Load-displacement curve of a DCB specimen at a displacement rate of 40 mm/s

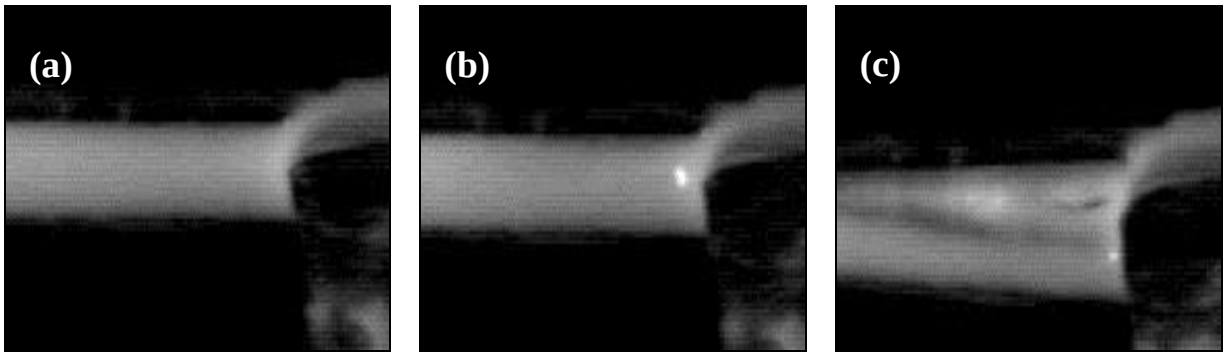

Figure 3. Fracture of STF was observed by HSD camera at dissected points of load-displacement curve in Fig. 2

By comparing the load-displacement curve of each specimen with corresponding video images, the critical load and the corresponding opening displacement for calculating the Mode-I fracture energy of the shear thickening fluid were defined. It was observed that not all DCB specimens showed the fracture behavior as a conventional solid. In particular, specimens tested at low displacement rates or with a thick layer of STF, exhibited an opening during which stretching of the STF with less

bending of the two CF/EP beams occurred. Additional calculation was done to get the effective Young's modulus of the CF/EP beams using the load-displacement curve and following the simple cantilever beam theory. For those DCB specimens, for which the effective Young's modulus of the CF/EP beam was clearly lower than that measured (using the same CF/EP laminate beam under three-point bending and following the procedure of ASTM D7264), the fracture energies calculated using Eq. (1) were excluded from the further discussion.

3.2. Effect of STF Thickness

It was expected that the STF layer thickness is a critical parameter, since the shear thickening phenomenon occurs only in localized regions where the shear rate goes beyond the critical shear rate, which is around 5/s [20]. Therefore the shear thickening effectiveness can disappear with increasing volume of the STF, especially at a reduced shear rate. The relation between the critical load to split the STF and the STF thickness is discerned in Fig. 4, with the STF thickness in a range from 0.2 mm to 2.05 mm. By arranging the maximum forces with respect to the STF thickness, it can be seen that a small STF thickness requires a greater load to split the STF in a DCB specimen, and vice versa. The greater the fluid thickness, the less aggregation or jamming of particles occurs, hence resulting in a lower critical load to split the specimen. However this relation is more obvious for low displacement rates (e.g., Fig. 4(a) for 5 mm/s and Fig. 4(b) for 10 mm/s). With increasing the displacement rate, the effect of the STF thickness on the critical load reduces. For displacement rates from 40 mm/s to 50 mm/s the critical load does not display any significant dependence on the STF thickness, Fig. 4(e) and Fig. 4(f).

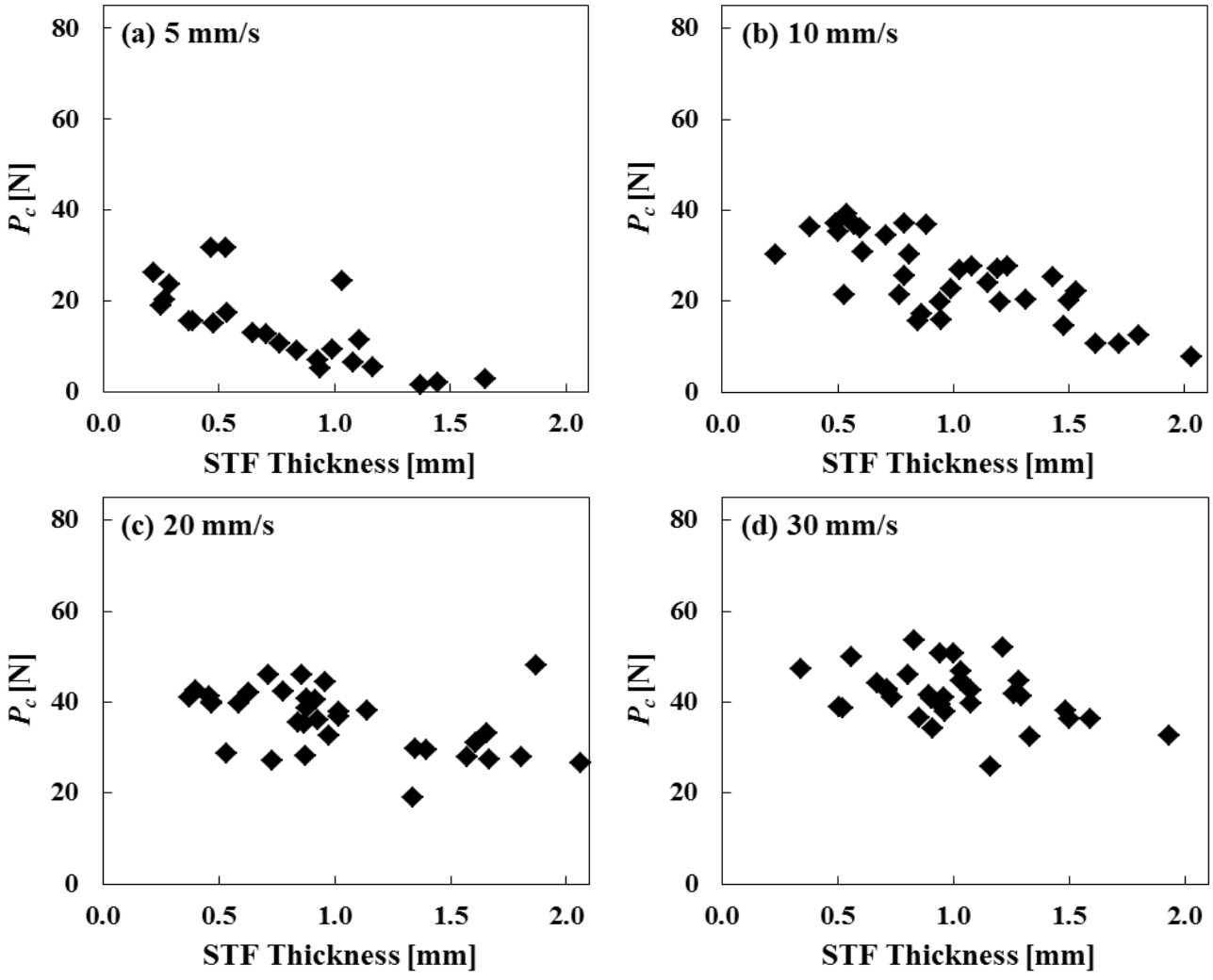

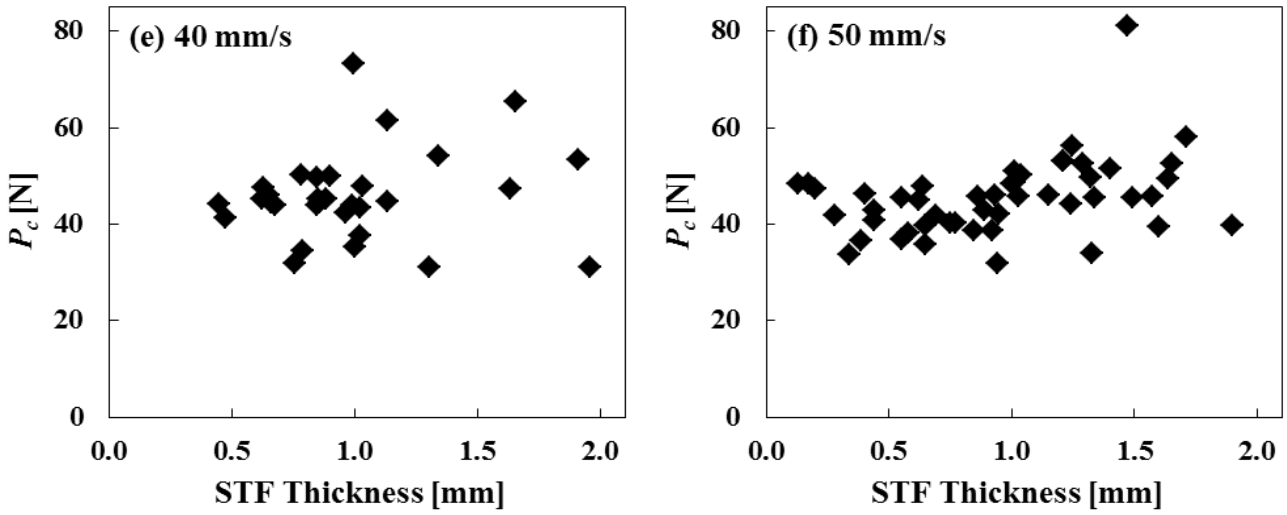

Figure 4. Effect of STF thickness on critical load at different displacement rates

Eq. (1) shows that the Mode-I fracture energy of STF is directly proportional to the critical load, and therefore, it is expected that a similar tread of Mode-I fracture energy in relation to the STF thickness exists. The Mode-I fracture energy versus the STF thickness is plotted for different displacement rates in Fig. 5.

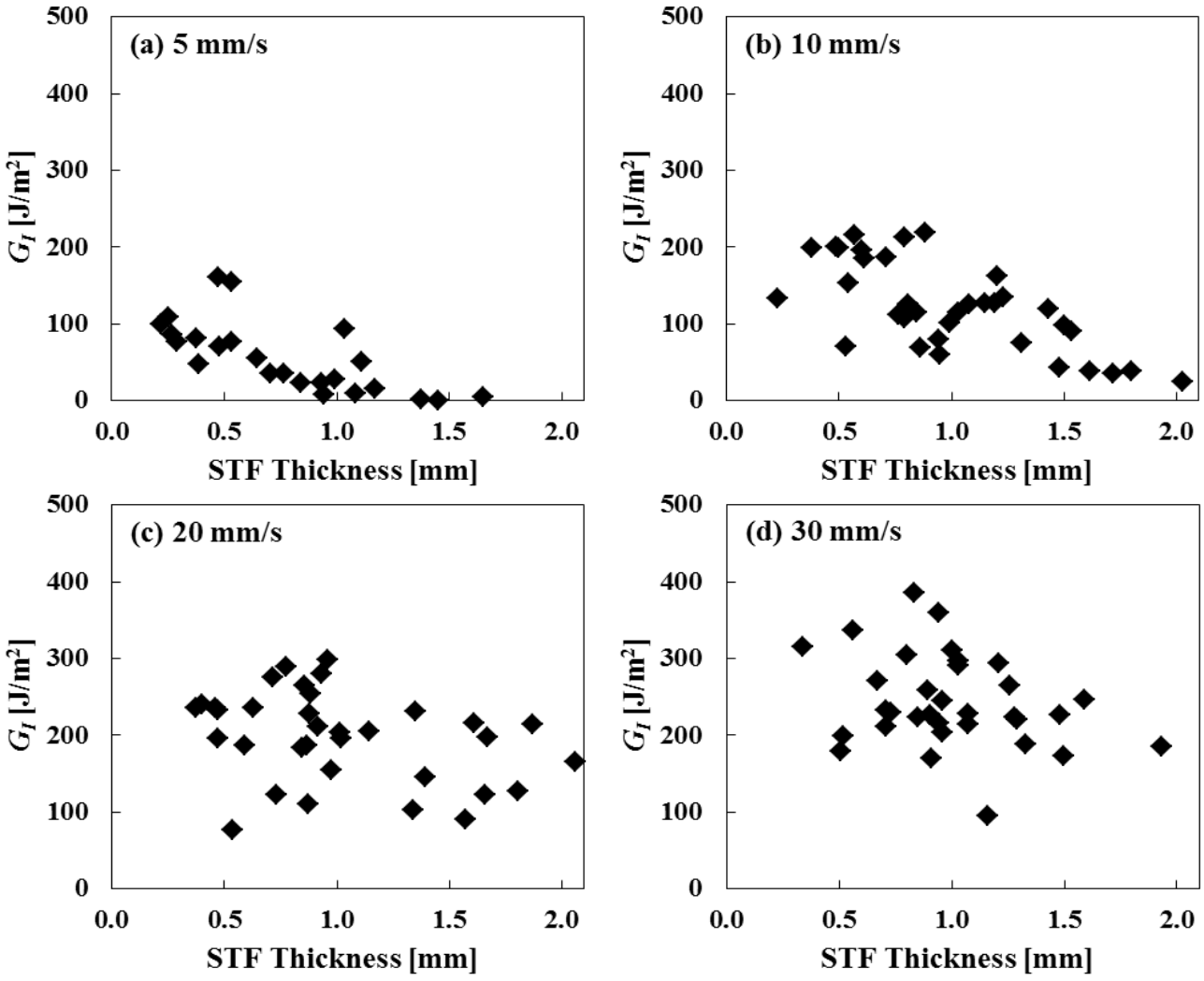

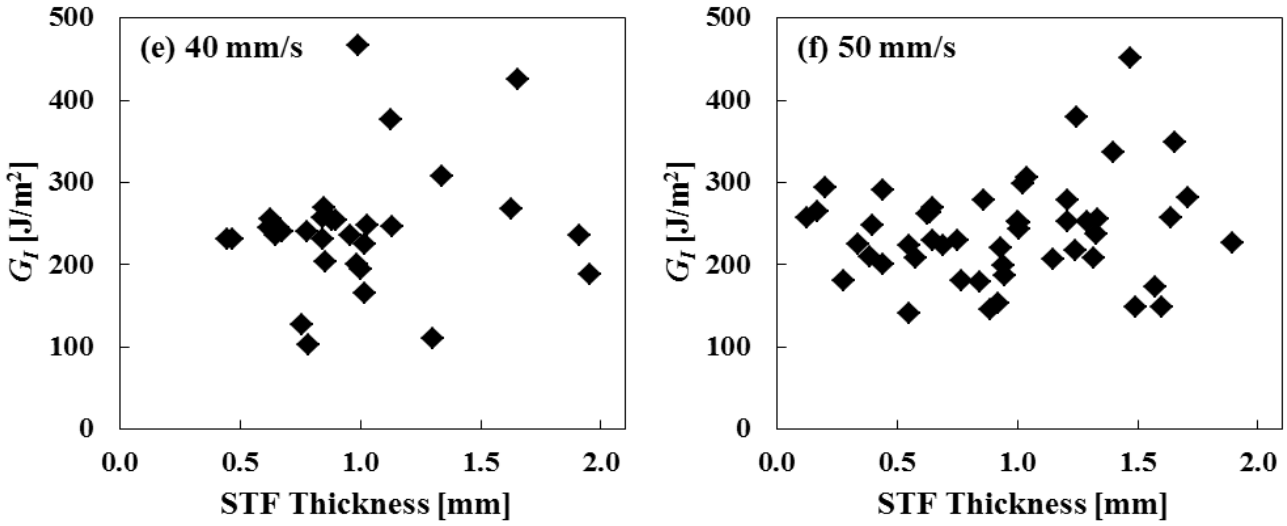

Figure 5. Effect of STF thickness on Mode-I fracture energy at different stroke rates

Up to a displacement rate of 20 mm/s, a reduced fracture energy with increased STF thickness is visible. This means, a larger STF thickness certainly results in a decreasing efficiency of the STF to absorb energy. However, with increasing the displacement rate this inverse relation cannot be observed anymore. For displacement rates from 30 to 50 mm/s, the Mode-I fracture energy does not show any significant relation with the STF thickness, in particular not at 50 mm/s.

3.3. Effect of Loading Rate

The loading or displacement rate is one of the most prominent parameters for examining the fracture behavior of STFs. The rates used here for the DCB fracture experiments were 1, 5, 10, 20, 30, 40, and 50 mm/s. The maximum of 50 mm/s was limited by the capacity of the Instron 8501 testing machine. The actual displacement rate was validated using the synchronized HSD images as well as the calculation from the time and displacement data. It was found that the actual displacement rates were very close to the preset ones in the testing range chosen. Existing differences were small, with a maximum being about ±4% of the preset ones.

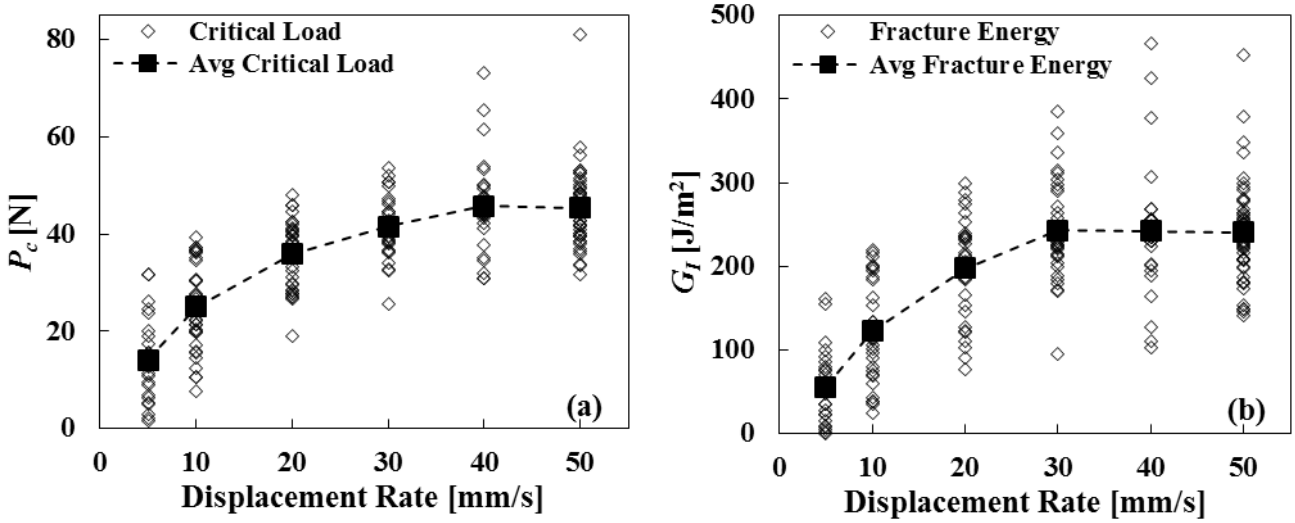

Figure 6. Effect of stroke speed on (a) critical load and (b) fracture energy of STF with different thickness

At a low displacement rate of 1 mm/s, STF is able to flow as an ordinary fluid, and the load cell did not measure any clear load with respect to the opening displacement, indicating such a

displacement rate is not enough for STF to have the transition from liquid to "solid". The HSD camera also shows there is no clear shear thickening effect of STF at this rate. In fact, before the displacement rate reaches 5 mm/s, STF did not show any "solid" like behavior, therefore no "fracture" was visible.

The effects of displacement rate on the critical load and fracture energy of the STF are graphically represented in Fig. 6, showing the results for each individual specimen. Fig. 6(a) presents the critical load with respect to displacement rate from 5 mm/s to 50 mm/s. With increasing deformation rate, the viscosity of the STF at the crack tip sharply increased, thus suppressing flow of the STF; instead it stiffens greatly and is capable of resisting an opening displacement more efficiently, causing a higher load. The increasing trend is supported by studies in the literature, which acknowledge a positive correlation between the STF's viscosity and the rate of deformation. The critical load varies with a substantial scatter for all displacement rates, because of the effect of STF thickness, articulated in the previous section. Other factors may also contribute to the scatter, such as voids or the uneven STF thickness because of leak of STF before the start of a test. However, the mean value of the critical load clearly increases with an increase in displacement rate up to 40 mm/s. A further increase in the displacement rate shows that the average critical load remains almost on a steady value. The mean values as well as the standard deviations of critical loads for different displacement rates are presented in Table 1.

Table 1. Means and standard deviations of critical load and fracture energy at different displacement rates

Displacement Rate [mm/s]	**Critical Load, P_c (Mean ± SD) [N]**	**Fracture Energy, G_I (Mean ± SD) [J/m^2]**
5	14 ± 9	56 ± 46
10	25 ± 9	123 ± 58
20	36 ± 7	198 ± 59
30	42 ± 6	243 ± 60
40	46 ± 9	242 ± 76
50	45 ± 8	240 ± 61

Almost a similar trend is observed for the Mode-I fracture energy of STF for different opening displacement rates in Fig. 6(b). As the critical load values, the fracture energy also shows a clear scatter in the values at each displacement rate, attributed to the effect of STF thickness. Also here, the average values and the standard deviations of fracture energy were calculated and summarized in Table 1. With an increase in the opening displacement rate, a positive relation is found between the fracture energy up to a displacement rate of 30 mm/s. At a low rate of 5 mm/s, the STF is able to absorb a small amount of energy while acting as a viscous "solid", though its actual value may be arguable. After the displacement rate reaches 30 mm/s the average fracture energy of STF is plateaued and remains almost constant with an averaged value about 240 J/m^2. This value indicates that the STF is capable of absorbing a certain amount of fracture energy, being comparable to a low cross-linked epoxy [23]. It seems the average value of Mode-I fracture energy of STF peaks at 30 mm/s, and it tends to reduce slightly after the displacement rate of 30 mm/s. However, such a tendency needs the careful evaluation of further studies, especially with facilities allowing higher displacement rates.

4. Conclusion

In this study, DCB specimens were used to characterize the fracture behavior and Mode-I fracture

energy of a shear thickening fluid (STF), containing 58 vol.% dispersion of styrene/acrylate particles in ethylene glycol. Effects of displacement rate (up to 50 mm/s) and STF thickness in the range of 0.2 to 2.05 mm were evaluated in detail.

The results reveal that as the displacement rate increases, the local shear rate at the crack-tip increases, sharply increasing the viscosity of the STF, thus suppressing the flow of the latter. It stiffens greatly and is capable of resisting an opening displacement efficiently, causing a higher load. Confirmed by the high speed camera images, STF clearly shows a "solid" behavior, fracturing with crack growth, when the opening displacement rate is higher than 20 mm/s. The Mode-I fracture energy of the STF increases with an increase in the displacement rate until 30 mm/s. In addition, the STF thickness was found to have a significant influence on the value of Mode-I fracture energy, attributed to the shear-thickening mechanism.

The most interesting result is that the STF adopted in this study shows almost a constant average value of fracture energy of 240 J/m^2 after the displacement rate is higher than 30 mm/s. This value indicates that the STF is capable of absorbing a certain amount of fracture energy, being comparable to a low cross-linked epoxy.

Future studies will be conducted at higher displacement rates. Such a more comprehensive characterization of the fracture behavior of STFs will certainly aid the development of energy absorbing devices using various STFs.

Acknowledgements

The authors acknowledge BASF AG (Germany) for providing the material. The authors would like to thank Trevor Shearing for his technical assistance and advice to carry out our test program. The project was partly supported by the University of Sydney Bridging Support Grant (Dr. Li Chang). M. Tabassum is grateful to the Australian Postgraduate Award (APA) and the top-up scholarship from the School of AMME, The University of Sydney.

References

[1] H. Barnes, "Shear-thickening ("dilatancy") in suspensions of nonaggregating solid particles dispersed in Newtonian liquids," *Journal of Rheology,* vol. 33, p. 329, 1989.

[2] R. Hoffman, "Discontinuous and dilatant viscosity behavior in concentrated suspensions. I. Observation of a flow instability," *Journal of Rheology,* vol. 16, p. 155, 1972.

[3] R. L. Hoffman, "Discontinuous and dilatant viscosity behavior in concentrated suspensions. II. Theory and experimental tests," *Journal of Colloid and Interface Science,* vol. 46, pp. 491-506, 1974.

[4] W. H. Boersma, J. Laven, and H. N. Stein, "Shear thickening (dilatancy) in concentrated dispersions," *AIChE journal,* vol. 36, pp. 321-332, 1990.

[5] R. L. Hoffman, "Explanations for the cause of shear thickening in concentrated colloidal suspensions," *Journal of Rheology,* vol. 42, p. 111, 1998.

[6] E. E. Bischoff White, M. Chellamuthu, and J. P. Rothstein, "Extensional rheology of a shear-thickening cornstarch and water suspension," *Rheologica acta,* vol. 49, pp. 119-129, 2010.

[7] F. J. Galindo-Rosales, F. J. Rubio-Hernández, and J. F. Velázquez-Navarro, "Shear-thickening behavior of Aerosil® R816 nanoparticles suspensions in polar organic liquids," *Rheologica acta,* vol. 48, pp. 699-708, 2009.

[8] N. J. Wagner and E. D. Wetzel, "Advanced body armor utilizing shear thickening fluids," ed: Google Patents, 2007.

[9] Y. S. Lee and N. J. Wagner, "Dynamic properties of shear thickening colloidal suspensions," *Rheol Acta,* vol. 42, pp. 199-208, 2003.

[10] Y. S. Lee, E. D. Wetzel, and N. J. Wagner, "The ballistic impact characteristics of Kevlar woven fabrics impregnated with a colloidal shear thickening fluid," *Journal of Materials Science,* vol. 38, pp. 2825 – 2833, 2003.

[11] E. D. Wetzel, Y. S. Lee, R. G. Egres, K. M. Kirkwood, J. E. Kirkwood, and N. J. Wagner, "The Effect of Rheological Parameters on the Ballistic Properties of Shear Thickening Fluid (STF)–Kevlar Composites," *NUMIFORM,* pp. 1-6, 2004.

[12] R. G. J. Egres, Y. S. Lee, J. E. Kirkwood, K. M. Kirkwood, E. D. Wetzel, and N. J. Wagner, ""Liquid armor": Protective fabrics utilizing shear thickening fluids," *IFAI 4th Int. Conf. on Safety and Protective Fabrics,* pp. 1-8, 2004.

[13] M. J. Decker, C. J. Halbach, C. H. Nam, N. J. Wagner, and E. D. Wetzel, "Stab resistance of shear thickening fluid (STF)-treated fabrics," *Composites Science and Technology,* vol. 67, pp. 565–578, 2007.

[14] J. M. Houghton, B. A. Schiffman, D. P. Kalman, E. D. Wetzel, and N. J. Wagner, "Hypodermic Needle Punture of Shear Thickening Fluid (STF)-Treated Fabrics," *Proceedings of SAMPE,* vol. 3, pp. 1-11, 2007.

[15] D. P. Kalman, J. B. Schein, J. M. Houghton, C. H. N. Laufer, E. D. Wetzel, and N. J. Wagner, "Polymer Dispersion Based Shear Thickening Fluid-Fabrics for Protective Applications," *Proceedings of SAMPE,* pp. 1-9, 2007.

[16] B. A. Rosen, C. H. N. Laufer, D. P. Kalman, E. D. Wetzel, and N. J. Wagner, "Multi-Threat Performance of Kaolin-Based Shear Thickening Fluid (STF)-Treated Fabrics," *Proceedings of SAMPE,* pp. 1-11, 2007.

[17] V. A. Grigoryan, I. F. Kobylkin, V. M. Marinin, and I. A. Bespalov, "Ballistic Performance of Textile Armor Treated with Shear Thickening Fluid," *Techniczne Wyroby Włókiennicze,* pp. 12-15, 2009.

[18] H. Laun, R. Bung, and F. Schmidt, "Rheology of extremely shear thickening polymer dispersions (passively viscosity switching fluids)," *Journal of Rheology,* vol. 35, p. 999, 1991.

[19] R. Helber, F. Doncker, and R. Bung, "Vibration attenuation by passive stiffness switching mounts," *Journal of sound and vibration,* vol. 138, pp. 47-57, 1990.

[20] L. Chang, K. Friedrich, A. Schlarb, R. Tanner, and L. Ye, "Shear-thickening behaviour of concentrated polymer dispersions under steady and oscillatory shear," *Journal of Materials Science,* vol. 46, pp. 339-346, 2011.

[21] ASTM, "Standard Test Method for Mode I Interlaminar Fracture Toughness of Unidirectional Fiber-Reinforced Polymer Matrix Composites," in *ASTM Annual Book of ASTM Standard D5528-94a* vol. 15.03, ed, 1999, pp. 283-292.

[22] J. Williams, "The fracture mechanics of delamination tests," *The Journal of strain analysis for engineering design,* vol. 24, pp. 207-214, 1989.

[23] S. Deng, L. Ye, and K. Friedrich, "Fracture behaviours of epoxy nanocomposites with nano-silica at low and elevated temperatures," *Journal of materials science,* vol. 42, pp. 2766-2774, 2007.